Deriving lung perfusion directly from CT image using deep convolutional neural network: A preliminary study

Abstract.
Functional avoidance radiation therapy for lung cancer patients aims to limit dose delivery to highly functional lung. However, the clinical functional imaging suffers from many shortcomings, including the need of exogenous contrast, longer processing time, etc. In this study, we present a new approach to derive the lung functional images, using a deep convolutional neural network to learn and exploit the underlying functional information in the CT image and generate functional perfusion image. In this study, ^{99m} Tc MAA SPECT/CT scans of 30 lung cancer patients were retrospectively analyzed. The CNN model was trained using randomly selected dataset of 25 patients and tested using the remaining 5 subjects. Our study showed that it is feasible to drive perfusion images from CT image. Using the deep neural network with discrete labels, the main defect regions can be predicted. This technique holds the promise to provide lung function images for image guided functional lung avoidance radiation therapy.

Keywords: Perfusion Imaging, Functional Avoidance Radiation Therapy, Deep Learning.

1 Introduction

Lung cancer is the most common occurring cancer among adults worldwide, with the most common cancer-related death (1.7 million in 2018) [1]. Approximately 85% of lung cancer patients were diagnosed with non-small cell lung cancer (NSCLC), of which 30%-50% were locally advanced (Stage III) NSCLC with median survival of 29 months[3]. The standard treatment for locally advanced NSCLC is concurrent chemoradiotherapy, but the long-term survival is impaired by a high rate of local failure[4]. The clinical practice to achieve local control is dose-escalation above the standard 60 Gy. However, giving more dose to the functional lung would increase the risk of radiation-induced lung injury, which involves radiation pneumonitis in the acute term and pulmonary fibrosis in the long term[5].

To avoid these side effects, functional avoidance radiation therapy for lung cancer patients was brought out to limit dose delivery to highly functional lung[6]. In this process, images with lung functional information was needed to differentiate function and non-function regions.

In clinical practice, the standard test of regional lung function were ventilation and perfusion imaging[7]. Clinical ventilation imaging, such as ^{99m}Tc SPECT[8], ^{68}Ga PET[9], and hyperpolarized ^{3}He gas MRI[10] are generally of low accessibility for the radiation oncology departments, invasive techniques, high cost. Therefore, clinical practice of these three modalities are limited. Deriving ventilation map from 4DCT

deformation fields also suffer from large variance from different registration algorithms[11].

Perfusion SPECT/CT imaging has been commonly utilized as a predictor of pulmonary function after surgery[12]. It also has potential for treatment planning in functional lung avoidance radiation therapy. Technetium-99m-labeled macro-aggregated albumin (^{99m} Tc MAA) provides a quantitative measure of regional variation in pulmonary perfusion. Besides perfusion SPECT imaging, a more convenient method is to derive the perfusion map from the CT images, which is a routinely utilized for radiation treatment planning. CT-based perfusion imaging does not require exogenous contrast anymore. This method is based on image processing of lung CT images acquired during tidal breathing or breath-hold procedures, and it should be able to transform CT from purely anatomic modality into one that can image and quantify lung perfusion. Since the CT Hounsfield Unit (HU) values is a function of the fractional air/tissue ratio[13], a deep learning model could hold the promise to extract the underlying information of translating the HU values into functional perfusion images. In the field of radiation therapy, deep learning-based convolutional neural network (CNN) has been successfully applied in low-dose CT image correction[14], MR-to-CT image synthesis[16], image segmentation[18], and so on. CNN has been found to be able to learn and exploit the underlying features that cannot be extracted by conventional image-processing methods[19]. CNN-based CT perfusion imaging has great promise to improve the toxicity outcomes of lung cancer radiation therapy by enabling perfusion-guided treatment planning that minimizes irradiation of functional lung.

This study aims to explore the feasibility of using deep neural network to derive perfusion-based pulmonary functional images from lung CT images. The proposed method utilized CNN to extract the air/tissue ratio information in the CT images and then used the underlying information to generate functional perfusion images. Our study showed that it is feasible to drive perfusion images from CT image. The performance of CNN with data discretization was superior over the CNN with data reduction by testing on our dataset. Given the performance of the preliminary study and computational efficiency of this method, the proposed deep learning method could hold significant value for future functional avoidance radiation therapy.

2 Materials and methods

2.1 Patients And Image Acquisition

In this study, ^{99m}Tc MAA SPECT/CT scans of 30 lung cancer patients were retrospectively analyzed. The use of the scan data and waivers of onset were approved by the Queen Mary Hospital (Hong Kong). Patients were immobilized in the supine position with the normal resting breathing. Each scan covered the whole lung volume. The CT images were reconstructed in 512×512 matrix with 0.977×0.977 mm^2 pixel spacing, and 1.25 mm slice spacing. The SPECT images were reconstructed in 128×128×128 matrix with 4.42×4.42×4.42 mm^3 voxel size. SPECT images were anatomically registered with the CT images.

2.2 Data Preprocessing

Image Preparation. Initially, SPECT images were resampled at the CT geometry. We built a lung mask to represent the lung parenchyma tissue. This mask included voxels of CT values < -300 HU growing from the lung region, and the trachea was manually excluded from the lung mask. For all cases, the primary lung tumor volume was not included from the lung mask. The lung mask was subsequently applied on the SPECT and CT images to segment the parenchyma volume. The segmented images were further cropped to include only the lung and resized to 128×128×64 matrix to reduce the consumption of the computation power. For both the SPECT and CT images, a 3D median filter within a cubic region of dimension 6×6×6 (cube width ~18 mm) was applied around each lung voxel for better feature selection.

Data Labelling. To normalize the SPECT values in different patients, all voxels values were divided by the 90th percentile value in the lung. Voxels with value of outlier were set with the threshold values. Our CNN was trained to derive the low function regions from the processed CT images so that the normal regions can be derived. Hence, we first obtained the training datasets consisting of paired input and output data. Since the purpose of this study was to predict the non-functional lung region.

Then, two labelling approaches were used to compare the performance of the network with different processed data. For the first scenario, voxels with values over 0.5 were excluded from the label map. The rest of the voxels were rescaled from 0 to 1. This method selected only a subset of the most important information from the SPECT images. For the second scenario, continuous values of the SPECT images were converted into 11 intervals with range of [0,0.1,0.2,… 1].

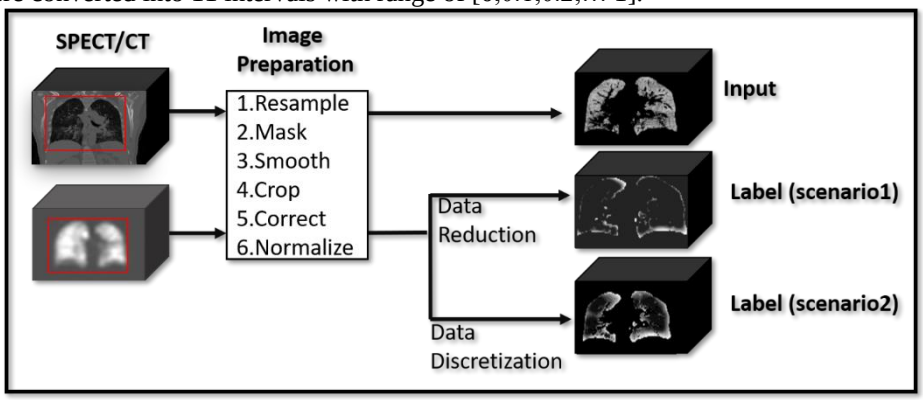

Fig. 1 Diagram of data preprocessing workflow.

2.3 Neural Network Architecture

We used a 3D U-net[20] based CNN to learn underlying information in the training phase and translate CT images into lung perfusion images in the testing phase. This

CNN includes 2 sequential paths (see Fig. 1). The contraction path, which captures the context in CT images, has 5 sequential layers. Each layer consists of a leaky rectified linear unit (leaky ReLU) as an activation function, followed by 3×3×3 convolution for detecting features, and 2×2×2 stride convolution for down-sampling. The expansion path, which enables precise localization, consists of the leaky ReLU, 3×3×3 convolution, 1×1×1 convolution, and 2×2×2 transpose convolution. The element-wise sum array layer was also used before the Sigmoid activation function to sum 3×3×3 convolution results of the previous layers. The predicted values are in the range of [0,1]. Symmetric skip connections (copy and concatenation), as shown in Figure 2, was used to translate the local details captured in the feature maps from the contraction path into the expansion path. The dropout and early stopping were used to avoid overfitting. This network was implemented using the Pytorch 1.1 framework.

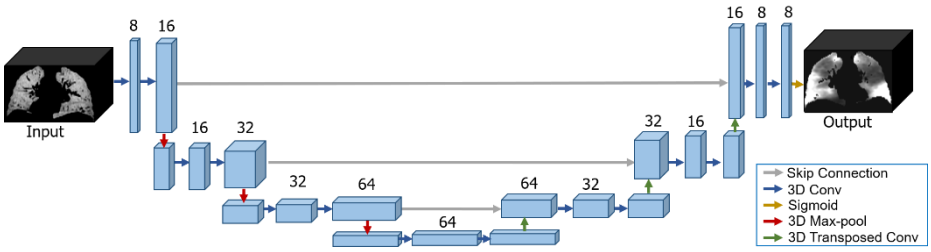

Fig. 2. CNN architecture. The blue indicates the feature map. Blue arrows represent three-dimensional (3D) convolutional layers with 3×3 filter. Red and green arrows indicate 3D max pooling and transposed convolution respectively. Orange arrow indicate sigmoid layer. The numbers on the top of the box indicate the number of channels.

2.4 Network Training

The network was trained using randomly selected dataset of 25 patients and tested using data from the remaining 5 subjects. Image flip was randomly applied to augment the training datasets during training. The processed CT and SPECT images were used for network training and validation. All the input and output datasets were in 3D volume format.

The mean square error was used as the loss function. Each layer was updated using error back-propagation with adaptive moment estimation optimizer (ADAM). The loss function used in this study was binary cross entropy. The learning rate for determining to what extent the newly acquired information overrides the old information was initially 10E-5. The number of epochs was 10000 and each epoch includes 2 iterations. The network was trained on one GTX 2080 TI GPU.

2.5 Evaluation

The generated perfusion images were compared with the perfusion label images from the testing groups. In this study, the correlation coefficient (Spearman's r) metric was used to compare the two images. The Spearman correlation coefficient *r* was defined using the following equation:

$$r = \frac{\sum_i (I_i - \bar{I})(I_i^* - \bar{I^*})}{\sqrt{\sum_i (I_i - \bar{I})^2 \sum_i (I_i^* - \bar{I^*})^2}} \quad (1)$$

where the notation I denotes the generated perfusion obtained using the network. I^* denotes perfusion label. The r values were in the range [-1,1] and represent the intensity monotonicity of spatially correlated voxels.

3 Results

For each testing case, we calculated the correlation coefficients of scenario 1 and scenario 2. Table 1 shows the correlation values of the prediction and labels. The average correlation value of scenario 1 is 0.53, which is larger than the average of scenario 2. Scenario 1 and scenario 2 have the same deviation. Considering that scenario 2 only predicts the functional lung regions, the correlation values is expected to be larger than those in scenario 1, which predicts the whole lung volume. This suggests the performance of CNN with data discretization is superior over the CNN with data reduction by testing on our data set. The correlations between the label and prediction demonstrated a moderate positive correlation for both scenarios.

Table 1. Correlation values between predicted and label images in 5 testing cases.

Case	1	2	3	4	5	Average ± S.D.
Scenario 1	0.45	0.65	0.32	0.63	0.62	0.53 ± 0.14
Scenario 2	0.18	0.43	0.37	0.51	0.42	0.39 ± 0.14

We also visualized two cases for qualitative analysis using the procedure mentioned in scenario 1. As shown in figure 3 and 4, most regions of the defects on the upper lobe of right lung were correctly labelled (red arrows). These images demonstrate good correspondence in the low/high function regions between the label and predicted image. For the data reduction case (Fig. 5), the defects on the lower lobe of right/left lung were not predicted. The result from qualitative analysis is in consistent with the correlation values, suggesting data discretization is superior over the data reduction by testing on our data set.

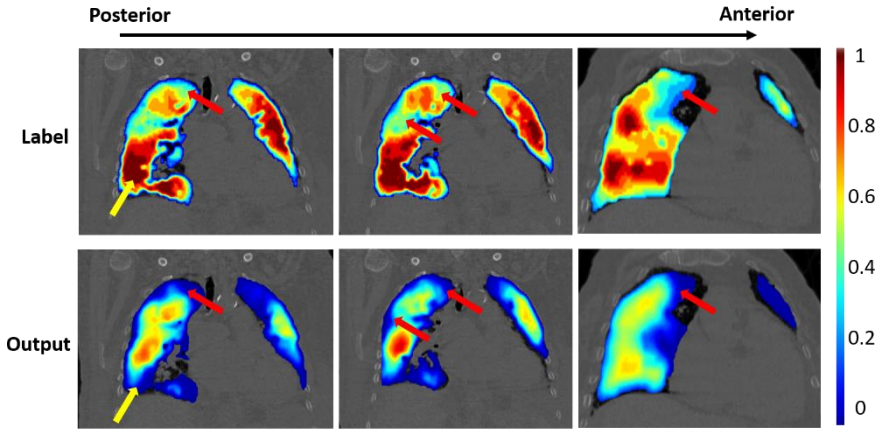

Fig. 3 Comparison of the discrete label and output of case 4 in scenario 1. All images have been normalized using the procedure mentioned in the method section. Red arrows indicate the correctly prediction. Yellow arrows indicate the incorrect prediction.

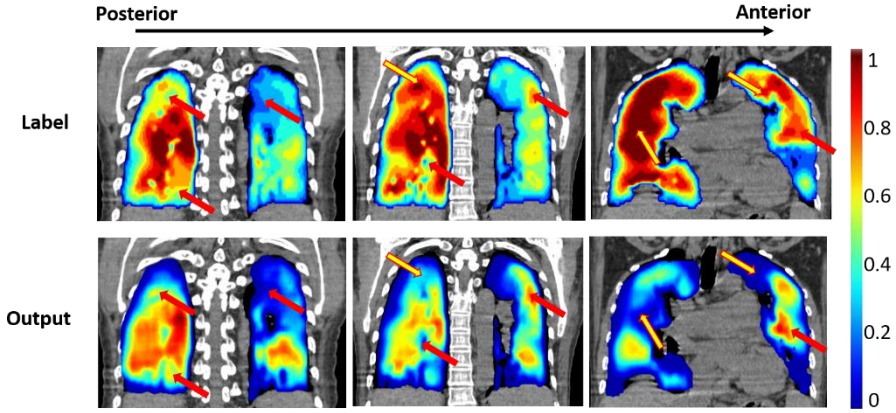

Fig. 4 Comparison of the label and output of case 5 in scenario 1. All images have been normalized using the procedure mentioned in the method section. Red arrows indicate the correctly prediction. Yellow arrows indicate the incorrect prediction.

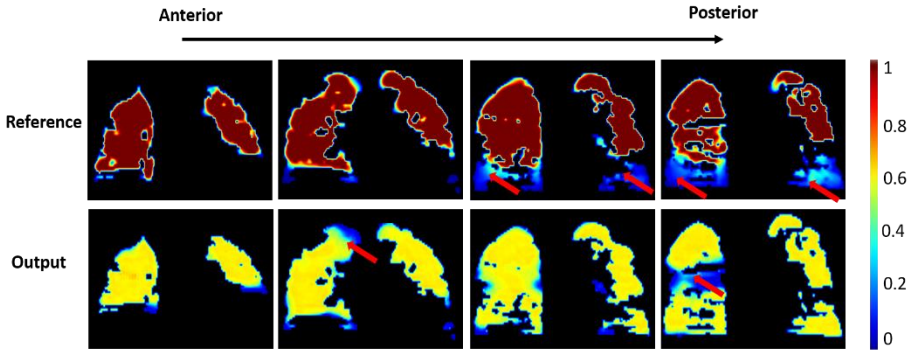

Fig. 5 Comparison of the reduced label and output of case 2 in scenario 2. All images have been normalized using the procedure mentioned in the method section. Red arrows indicate the clinical defect regions.

4 Summary

Our preliminary study successfully demonstrated the feasibility to drive perfusion images from single phase CT image. Using the deep neural network with discrete data, the main defect regions can be predicted. This technique holds the promise to provide lung functional images for functional lung avoidance radiation therapy.

References

1. Ferlay, J., et al., *Estimating the global cancer incidence and mortality in 2018: GLOBOCAN sources and methods.* Int J Cancer, 2019. **144**(8): p. 1941-1953.
2. Midha, A., S. Dearden, and R. McCormack, *EGFR mutation incidence in non-small-cell lung cancer of adenocarcinoma histology: a systematic review and global map by ethnicity (mutMapII).* Am J Cancer Res, 2015. **5**(9): p. 2892-911.
3. Bradley, J.D., et al., *Standard-dose versus high-dose conformal radiotherapy with concurrent and consolidation carboplatin plus paclitaxel with or without cetuximab for patients with stage IIIA or IIIB non-small-cell lung cancer (RTOG 0617): a randomised, two-by-two factorial phase 3 study.* Lancet Oncol, 2015. **16**(2): p. 187-99.
4. Lee, E., et al., *Functional lung avoidance and response-adaptive escalation (FLARE) RT: Multimodality plan dosimetry of a precision radiation oncology strategy.* Med Phys, 2017. **44**(7): p. 3418-3429.
5. Madani, I., et al., *Predicting risk of radiation-induced lung injury.* J Thorac Oncol, 2007. **2**(9): p. 864-74.
6. Hoover, D.A., et al., *Functional lung avoidance for individualized radiotherapy (FLAIR): study protocol for a randomized, double-blind clinical trial.* BMC Cancer, 2014. **14**: p. 934.

7. Harders, S.W., S. Balyasnikowa, and B.M. Fischer, *Functional imaging in lung cancer.* Clin Physiol Funct Imaging, 2014. **34**(5): p. 340-55.
8. Suga, K., *Technical and analytical advances in pulmonary ventilation SPECT with xenon-133 gas and Tc-99m-Technegas.* Annals of Nuclear Medicine, 2002. **16**(5): p. 303-310.
9. Callahan, J., et al., *High-resolution imaging of pulmonary ventilation and perfusion with 68Ga-VQ respiratory gated (4-D) PET/CT.* Eur J Nucl Med Mol Imaging, 2014. **41**(2): p. 343-9.
10. Mathew, L., et al., *Hyperpolarized (3)He magnetic resonance imaging: comparison with four-dimensional x-ray computed tomography imaging in lung cancer.* Acad Radiol, 2012. **19**(12): p. 1546-53.
11. Kipritidis, J., et al., *The VAMPIRE challenge: A multi-institutional validation study of CT ventilation imaging.* Medical Physics, 2019. **46**(3): p. 1198-1217.
12. Gefter, W.B. and H. Hatabu, *Functional lung imaging: emerging methods to visualize regional pulmonary physiology.* Acad Radiol, 2003. **10**(10): p. 1085-9.
13. Kipritidis, J., et al., *Estimating lung ventilation directly from 4D CT Hounsfield unit values.* Med Phys, 2016. **43**(1): p. 33.
14. Chen, H., et al., *Low-Dose CT With a Residual Encoder-Decoder Convolutional Neural Network.* IEEE Trans Med Imaging, 2017. **36**(12): p. 2524-2535.
15. Wolterink, J.M., et al., *Generative Adversarial Networks for Noise Reduction in Low-Dose CT.* IEEE Trans Med Imaging, 2017. **36**(12): p. 2536-2545.
16. Jin, C.B., et al., *Deep CT to MR Synthesis Using Paired and Unpaired Data.* Sensors, 2019. **19**(10).
17. Leung, K., et al., *A deep-learning-based fully automated segmentation approach to delineate tumors in FDG-PET images of patients with lung cancer.* Journal of Nuclear Medicine, 2018. **59**.
18. Shin, H.C., et al., *Deep Convolutional Neural Networks for Computer-Aided Detection: CNN Architectures, Dataset Characteristics and Transfer Learning.* Ieee Transactions on Medical Imaging, 2016. **35**(5): p. 1285-1298.
19. Zhong, Y., et al., *Technical Note: Deriving ventilation imaging from 4DCT by deep convolutional neural network.* Med Phys, 2019. **46**(5): p. 2323-2329.
20. Ronneberger, O., P. Fischer, and T. Brox, *U-Net: Convolutional Networks for Biomedical Image Segmentation.* Medical Image Computing and Computer-Assisted Intervention, Pt Iii, 2015. **9351**: p. 234-241.